H1prelim-21-031
April 8, 2021

Measurement of lepton-jet correlations in high Q^2 neutral-current DIS with the H1 detector at HERA

The H1 Collaboration

Abstract

A measurement of jet production in high Q^2 neutral-current DIS events close to the Born-level configuration $\gamma^* q \to q$ (Born kinematics) is presented. This cross section is measured deferentially as a function of the jet transverse momentum and pseudorapidity, as well as lepton-jet momentum imbalance and azimuthal angle correlation. The jets are reconstructed in the laboratory frame with the k_T algorithm and a distance parameter of 1.0. The data are corrected for detector effects using the OMNIFOLD method, which incorporates a simultaneous and unbinned unfolding in four dimensions using machine learning. The results are compared with leading order Mont Carlo event generators and higher order calculations performed within the context of collinear or transverse-momentum-dependent (TMD) factorization in Quantum Chromodynamics (QCD). The measurement probes a wide range of QCD phenomena, including TMD parton-distribution functions (PDFs) and their evolution with energy.

1 Introduction

The multi-dimentional structure of the proton is encoded in transverse-momentum-dependent and generalized parton-density functions (TMDs and GPDs, respectively). These are related to the the proton Wigner distribution – the six-dimensional quantum-phase density – which provides a complete description of the proton wave function in terms of quarks and gluons [1]. Knowledge of the TMDs, the GPDs, and ultimately the Wigner function will help to reveal the origin of the proton's spin, mass, size, and other properties.

By studying TMD physics we also seek to unravel rich, unexplored aspects of Quantum Chromodynamics (QCD). For example, TMD functions do not follow the standard DGLAP evolution equations [2–4] but rather a more complex set of equations that involve non-perturbative kernels. Lattice calculations have made significant advances in the calculation of the TMD-evolution "Collins-Soper" kernel [5, 6]. However, the subject of TMD evolution remains an open question in part because of the lack of data.

Measurements in DIS that target TMD physics have been mainly performed at fixed-target experiments, such as HERMES at DESY, COMPASS at CERN, and CLAS at JLab; see Ref. [7] for a recent review. These studies have focused on polarized and unpolarized semi-inclusive DIS (SIDIS) with one or two hadrons being measured. A key limitation of SIDIS cross-section measurements is that they only constrain the convolution of TMD parton distribution functions and TMD fragmentation functions (TMD PDFs and TMD FFs, respectively). This convolution naturally leads to near-maximal correlations on the TMD-PDF and TMD-FF parameters extracted from SIDIS data. This issue can in part be alleviated with global analyses that include e^+e^- or Drell-Yan data [8]. However, those typically cover different kinematic regions, such that issues of TMD-evolution, TMD factorization, and TMD universality complicate these studies.

Jet measurements targeting TMD physics were pioneered at RHIC. For example, studies of jets produced in polarized proton-proton collisions probe the Sivers [9–11], transversity, and Collins TMD functions [12–14]. Measurements of jet fragmentation in unpolarized proton collisions have targeted TMD fragmentation functions [15]. Recently, jet production in DIS was proposed as a key channel for TMD studies [16–19]. The Born-level configuration, $\gamma^* q \to q$, is key to access the quark TMD sector [16–18, 20, 21].

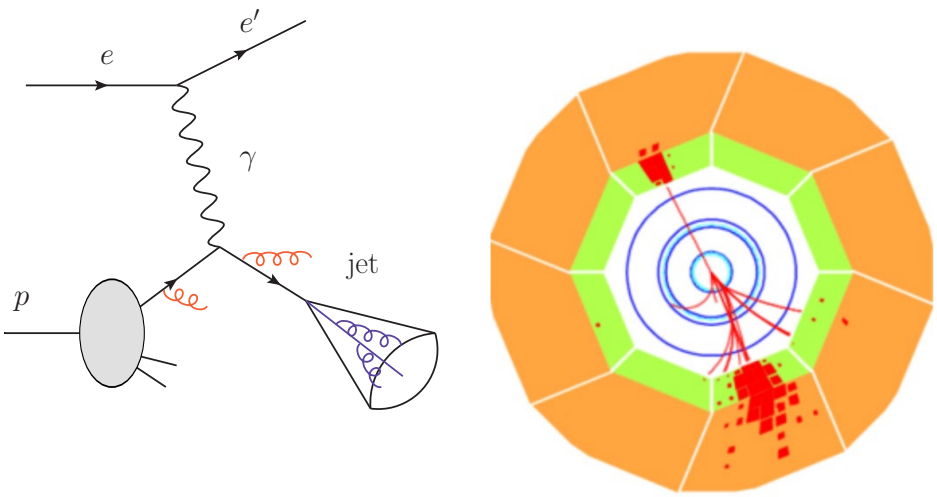

Fig. 1: Left: Illustration of the neutral-current DIS process at Born kinematics. Event display of a high Q^2 DIS event with approximate Born kinematics.

Measurements of jet production in DIS, probing the kinematics of the Born-level configuration (Born

kinematics), have not received much experimental attention so far. In fact, the bulk of the previous DIS jet measurements at HERA targeted gluon-initiated processes by requiring large transverse momentum in the Breit frame [22]. This requirement suppresses the Born kinematics, which is often referred to as "quark-parton-model background". There are two possibilities to measure the Born kinematics in jet production in DIS, which is illustrated in figure 1. The first possibility [16,17] includes a jet clustering in the Breit frame, where jets are required to have low transverse momentum p_{T}, which demands the use of dedicated jet algorithms such as Centauro [23]. The second possibility [18,21] involves jets reconstructed in the laboratory rest frame.

The TMD evolution is largely unconstrained and its impact on several observables is still being debated. One of the reasons is a gap in the coverage in virtuality Q^2 of existing measurements. Most of the DIS measurements provide data at low Q^2 (≈ 1 GeV^2) from fixed-target experiments. Drell-Yan production in fixed-target and collider experiments can provide TMD-sensitive measurements up to high Q^2 (≈ 10000 GeV^2). However, a global interpretation is complicated because of issues with TMD universality and a breakdown of TMD factorization in hadron-hadron collisions. In this note, measurements are presented which bridge this gap by studying TMD-sensitive observables in DIS at higher Q^2 than what can be reached with fixed-target experiments.

2 Data and Simulation

Data used for this analysis were collected with the H1 detector [24] in the years 2006 and 2007 when positrons and protons were collided at energies of 27.6 GeV and 920 GeV, respectively. The total integrated luminsosity of this data sample corresponds to 136 pb^{-1}. The DJANGOH [25] 1.4 and RAPGAP [26] 3.1 event generators, combined with a detailed simulation of the H1 detector response based on the GEANT3 simulation program [27], are used for corrections of detector effects.

3 Event Selection

This analysis follows the event selection that was used in previous H1 measurements of jets in high-Q^2 neutral-current DIS events [28]. The Σ method [29] is used to reconstruct the DIS variables, as:

$$
\begin{aligned}
y &= \frac{\sum_{i\in had}(E_i - p_{i,z})}{\sum_{i\in had}(E_i - p_{i,z}) + E_{e'}(1-\cos\theta_{e'})} \\
Q^2 &= \frac{E_{e'}\sin^2\theta_{e'}}{1-y},
\end{aligned}
$$

where $E_{e'}$ and $\theta_{e'}$ are the energy and polar angle of the scattered lepton; $\sum_{i\in had}(E_i - p_{i,z})$ is the total difference between the energy and longitudinal momentum of the entire hadronic-final state (HFS). An energy-flow algorithm [30,31] is used to define the HFS objects that enter the sum $\sum_{i\in had}$.

Events with $Q^2 > 150$ GeV^2 and $0.08 < y < 0.7$ are selected for further analysis. The trigger used to select NC DIS events requires a cluster in the electromagnetic part of the LAr calorimeter. After fiducial cuts, the trigger efficiency is higher than 99.5% [32,33] for scattered electron candidates with energy $E'_e > 11$ GeV for the inclusive NC DIS sample. Further fiducial and quality cuts are discussed in Ref. [33].

4 Definition of observables

The following four observables are simultaneously measured:

– the jet transverse momentum in the laboratory frame, $p_{\mathrm{T}}^{\mathrm{jet}}$,

– the jet pseudorapidity in the laboratory frame, $\eta^{\text{jet}}_{\text{lab}}$,

– the azimuthal angle correlation between the scattered lepton and the jet, $\Delta\phi = \pi - (|\phi^e - \phi^{\text{jet}}| \bmod \pi)$,

– the momentum imbalance between the electron and the jet, $q_T = |\vec{p}^{\,e}_T + \vec{p}^{\,\text{jet}}_T|$.

The cross-section measurement is normalized to the inclusive jet cross-section integrated over the the fiducial phase space defined in Section 6.

The aim of this measurement is to probe back-to-back lepton-jet production:

$$e + p \to e + \text{jet}(q_T) + X\,. \tag{1}$$

The TMD framework is formally applicable for $q_T \ll Q$ [18]. Typical TMD phenomenological analyses use a cut-off of $q_T/Q < 0.25$–0.75 [34]. Measurements of q_T over a wide range can probe the transition between the TMD regime and the collinear QCD regime; the "matching" between the two frameworks is an open problem [35].

5 Jet reconstruction

The Fastjet 3.3.2 package [36, 37] is used to cluster jets in the laboratory frame with the inclusive k_T algorithm [38, 39] and distance parameter $R = 1.0$. The inputs for the jet clustering are HFS objects with $-1.5 < \eta_{\text{lab}} < 2.75$.

Jets with transverse momentum $p^{\text{jet}}_{\text{T}} > 5$ GeV and pseudorapidity in the laboratory frame $-1.5 < \eta^{\text{jet}}_{\text{lab}} < 2.75$ are selected for further analysis. This selection ensures that jets are well contained in the LAr calorimeter.

The input for the jet clustering at the generator level ("truth-level") are final-state particles with $c\tau > 10$ mm generated with RAPGAP or DJANGOH, excluding the scattered lepton and neutrinos. Reconstructed jets are matched to the generated jets with an angular-distance selection of

$$\Delta R = \sqrt{(\phi^{\text{jet}}_{\text{gen}} - \phi^{\text{jet}}_{\text{reco}})^2 + (\eta^{\text{jet}}_{\text{gen}} - \eta^{\text{jet}}_{\text{reco}})^2} < 0.9. \tag{2}$$

6 Fiducial region definition

The fiducial phase space used to define the cross-sections is $p^{\text{jet}}_{\text{T}} > 10$ GeV, $-1.0 < \eta^{\text{jet}}_{\text{lab}} < 2.5$, $Q^2 > 150$ GeV^2 and $0.2 < y < 0.7$. The phase space used to select events and reconstructed jets is larger to account for bin migrations in and out of the fiducial region and mitigate acceptance effects: $p^{\text{jet}}_{\text{T}} > 5$ GeV, $-1.5 < \eta^{\text{jet}}_{\text{lab}} < 2.75$, $0.08 < y < 0.7$ and $Q^2 > 150$ GeV^2.

7 Unfolding with OMNIFOLD

The most widely used unfolding methods are based on various forms of regularized matrix inversion [40–42]. While highly successful, an important limitation of these approaches is that the binning of the observables must be fixed at the start of the measurement and this also typically limits the number of observables that are simultaneously unfolded.

A variety of alternative unfolding methods have been proposed to solve these challenges. For example, some proposals avoid binning [43–47] and others use machine learning to improve various aspects of the measurement precision [45–49]. However, these proposals are untenable in high dimensions and/or do not reduce to standard methods in the binned case. For this reason, we use the OMNIFOLD method [50]

to perform the first high-dimensional and unbinned measurement. OMNIFOLD formally reduces to the widely studied iterative Bayesian[1] unfolding approach [40] when the inputs are binned. Furthermore, it uses reweighting instead of direct generative modeling, so the neural networks need to only learn small corrections to the simulation instead of learning the full probability density of the data.

Figure 2 illustrates the OMNIFOLD approach. First, weights are derived to match the detector-level simulation with data. In simulation, there is a match between particle-level and detector-level events and so the particle-level collisions inherit ('pull') the detector-level weights. The resulting weights are not a proper function of the phase space because two identical particle-level events can be mapped to different detector-level events. Step two of OMNIFOLD then learns a set of weights between the nominal particle-level simulation and the weighted particle-level simulation. These weights are designed to be a function of the particle-level phase space. The particle-level weights can then be inherited by the detector-level events ('pushed') and the entire process is repeated n times. Neural networks are used as reweighting functions because they are naturally unbinned and can readily process high-dimensional features. These networks are implemented in KERAS [53] and TENSORFLOW [54] using the ADAM [55] optimization algorithm.

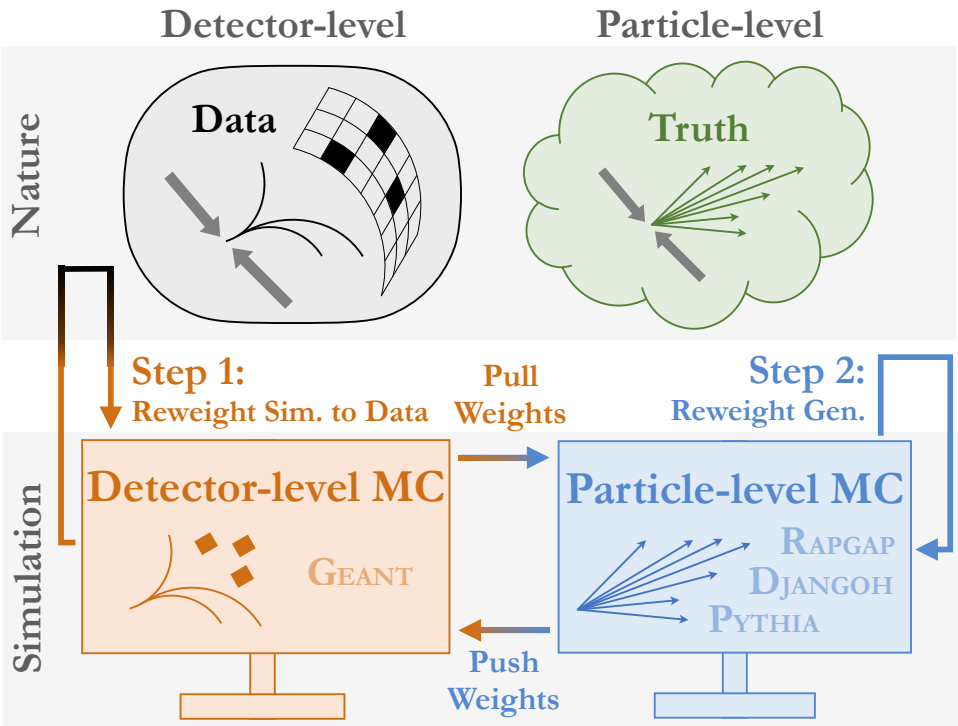

Fig. 2: An illustration of the OMNIFOLD method. Figure adapted from Ref. [50].

8 Closure tests

We perform "closure tests" by using either RAPGAP or DJANGOH events to create a pseudo-dataset, which we unfold using the method described in section 7 just like the data. We then compare the unfolded pseudo-data with the truth-level distributions to estimate the degree of bias introduced by the unfolding procedure. The RAPGAP and DJANGOH distributions "bracket" the data and have rather different underlying models. Therefore, this closure test provides a realistic evaluation of the procedure bias. We perform this closure test twice: one using DJANGOH for the pseudo-data and the other using RAPGAP. Both ways yield similar closure and only one is shown below.

[1] Also called Lucy-Richardson deconvolution [51, 52].

Figure 3 shows the comparison between the unfolded pseudo-data and the corresponding truth-level distributions. The test shows a relatively small residual bias from the prior distributions, which is shown with the RAPGAP/DJANGOH ratio (red line). The level of non-closure is within $\pm 10\%$ for all observables, and is much smaller for most kinematic intervals.

9 Theoretical models

The measured cross sections are compared to the predictions described in the following.

– **High-order collinear pQCD calculation:**
The calculation at next-to-next-to-leading order (NNLO) accuracy in QCD was obtained with the POLDIS code [56, 57], which is based on the Projection to Born Method [58]. The POLDIS code combines the computation for di-jet production in DIS at NLO with the NNLO DIS structure functions, allowing for a calculation of fully-exclusive single jet observables with NNLO accuracy in polarized and unpolarized DIS. These calculations are multiplied by a hadronization correction that is obtained with PYTHIA8.3, as described in section 10. The uncertainty of the calculations are obtained using the standard scale-variation procedure.

– **TMD-framework calculation:**
The TMD calculation uses the framework developed in Refs. [18, 21]. As input, it uses the TMD PDFs and soft functions derived in Ref. [59]. This has been recently tested in a global TMD analysis [34]. The calculation is performed at the NLL$'$ (next-to-leading logarithmic) accuracy. Depending on the convention this can also be labelled NLO+NLL accuracy. This calculation is purely performed within TMD factorization and no matching to the high q_T region is included, where the TMD approach is expected to break down. In contrast to pQCD calculations, the TMD calculations do not require non-perturbative corrections, because such effects are already included. Calculations with the TMD framework are available for the TMD-sensitive cross-sections, which are q_T/Q and $\Delta\phi$, but not for the $p_{\mathrm{T}}^{\mathrm{jet}}$ and $\eta_{\mathrm{lab}}^{\mathrm{jet}}$ cross-sections. Uncertainties are not yet available for the TMD predictions[2].

– **Monte-Carlo generators:**
The RAPGAP [26], and DJANGOH [25] MC generators implement Born-level matrix elements for the NC DIS, boson–gluon fusion and QCD Compton processes. DJANGOH [25], uses the Colour Dipole Model as implemented in Ariadne [60] for higher order emissions, and Rapgap [26] uses parton showers in the leading-logarithmic approximation. Both the RAPGAP and DJANGOH simulations use the CTEQ6L LO PDF set [61] and the Lund hadronization model [62].

The PYTHIA8.3 [63, 64] event generator is used to model NC DIS events with Born-level matrix elements coupled with a parton shower, the NNPDF2.3 QCD+QED LO PDF set [65], and the Lund hadronization model [62].

The CASCADE [66] is an event generator based on TMD parton densities, and in incorporates TMD parton showers and hadronization. The calculations shown in this note use the KATIE program [67] to obtain the off shell matrix element ($e + q^* \to e' + q$) with the parton-branching (PB) TMD PDFs [68–70]. The output of KATIE is used as input to CASCADE to add final-state radiation and hadronization effects. Two different calculations are produced: one with the PB-TMD-set1, which if integrated corresponds to HERAPDF2.0 [71], and PB-TMD-set2, which has angular ordering and p_T in the scale in α_s. The PB-TMD-set2 has been shown to work well to describe Z production at the LHC and at low energies [72, 73].

[2] The scale-variation procedure that is standard in the collinear framework does not translate easily to the TMD framework.

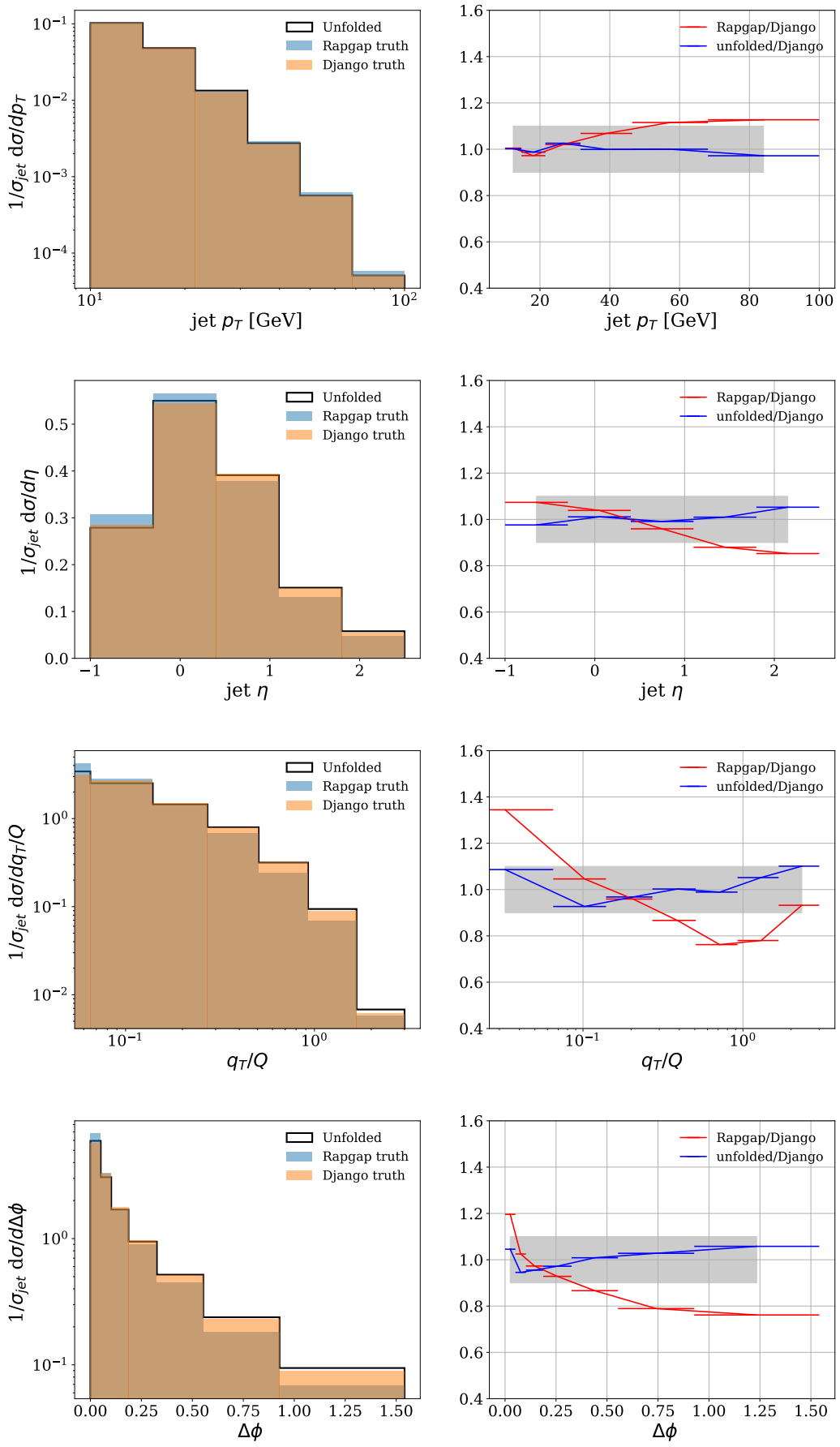

Fig. 3: Closure test results. Here, RAPGAP is used to obtain the response and DJANGOH is used as pseudo-data. The closure test is defined in the phase-space $Q^2 > 150$ GeV^2, $0.2 < y < 0.7$ and $p_{\mathrm{T}}^{\mathrm{jet}} > 10$ GeV at the truth level.

This measurement employs the Σ reconstruction method [29], which is insensitive to initial-state QED radiation. Virtual higher-order QED and electroweak effects cancel in the cross section ratios. Therefore, the measurements can be compared to QED born-level predictions. This procedure is expected to be accurate below the percent level.

10 Hadronization Corrections

Hadronization corrections are applied to the parton-level pQCD calculations when comparing these to data. We estimated these corrections using PYTHIA8.3 [74] with its default parameters. Events are selected if they are generated in the fiducial region, as defined in section 5. Jets are reconstructed with the same parameters as described in section 5. The hadronization corrections are derived as the ratio of distributions obtained with the hadronization step switched on, to the ones obtained with the hadronization step switched off.

Figure 4 shows the distributions obtained for $p_{\mathrm{T}}^{\mathrm{jet}}$, $\eta_{\mathrm{lab}}^{\mathrm{jet}}$,$q_T/Q$ and $\Delta\phi$ and the corresponding ratios. The hadronization corrections for the $p_{\mathrm{T}}^{\mathrm{jet}}$ observable are within 5% of unity and do not show a systematic pattern. In contrast, the hadronization corrections for $\eta_{\mathrm{lab}}^{\mathrm{jet}}$ are about 0.9 at $\eta_{\mathrm{lab}}^{\mathrm{jet}} > 1.0$ and increase up to 20% with decreasing $\eta_{\mathrm{lab}}^{\mathrm{jet}}$. The hadronization corrections as a function of q_T/Q are smaller than 5% for values smaller than 0.3 and increase to about 10% for high values. A similar behaviour is obtained for the corrections as a function of $\Delta\phi$.

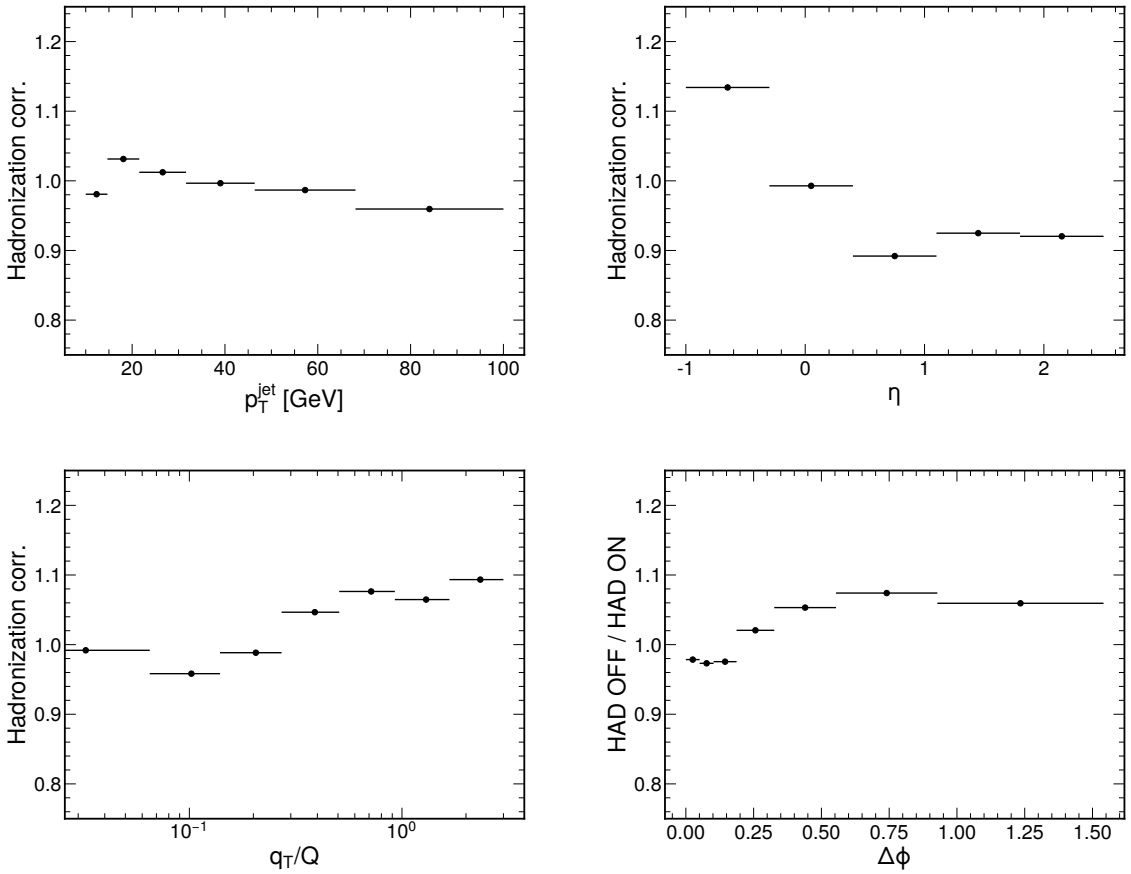

Fig. 4: Hadronization correction (i.e. ratio of cross-sections with and without hadronization step), which is calculated using PYTHIA8.3 .

11 Results

Figures 5 and 6 show the measured cross-sections as a function of jet transverse momentum, lepton-jet balance and lepton-jet azimuthal correlations, which are compared to analytical calculations and predictions obtained with event generators, respectively. The unfolding is performed simultaneously in four dimensions and is unbinned, but the results are presented as four separate histograms to quantitatively compare to predictions.

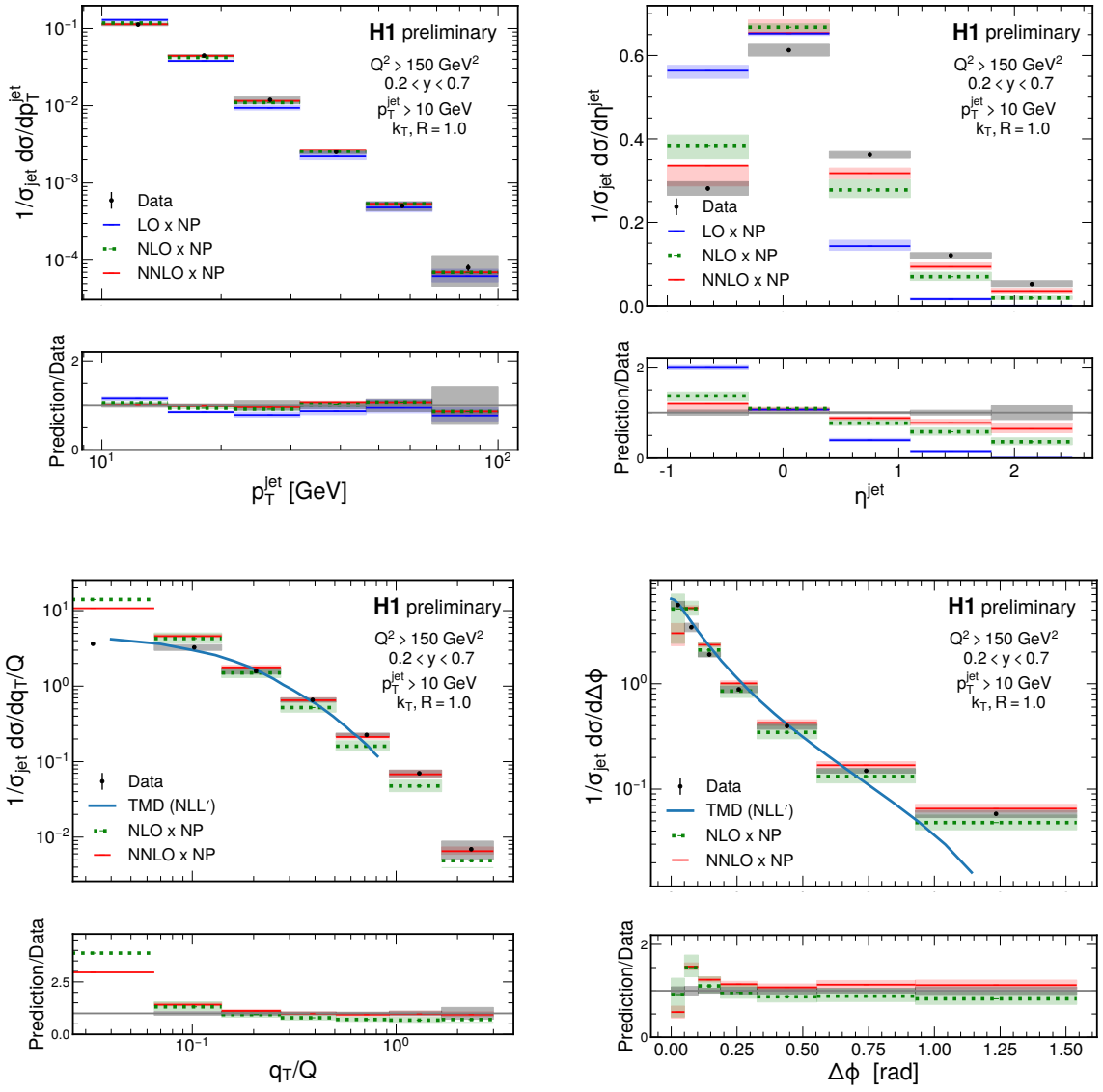

Fig. 5: Measured cross-sections, normalized to the inclusive jet production cross section, as a function of the jet transverse momentum, jet pseudorapidity, lepton-jet momentum balance, and lepton-jet azimuthal angle correlation. Predictions obtained with the pQCD (corrected by hadronization effects, "NP") are shown as well. Predictions obtained with the TMD framework are shown for the q_T/Q and $\Delta\phi$ cross-sections. At the bottom, the ratio between pQCD predictions and the data are shown (the TMD NLL$'$ calculations are not included). The gray bands represent the total systematic uncertainty of the data; the bars represent the statistical uncertainty of the data, which is typically smaller than the marker size. The color bands represent the uncertainty on the pQCD calculations.

The p_T^{jet} cross-section is described within uncertainties by the NNLO calculation; the discrepancies with

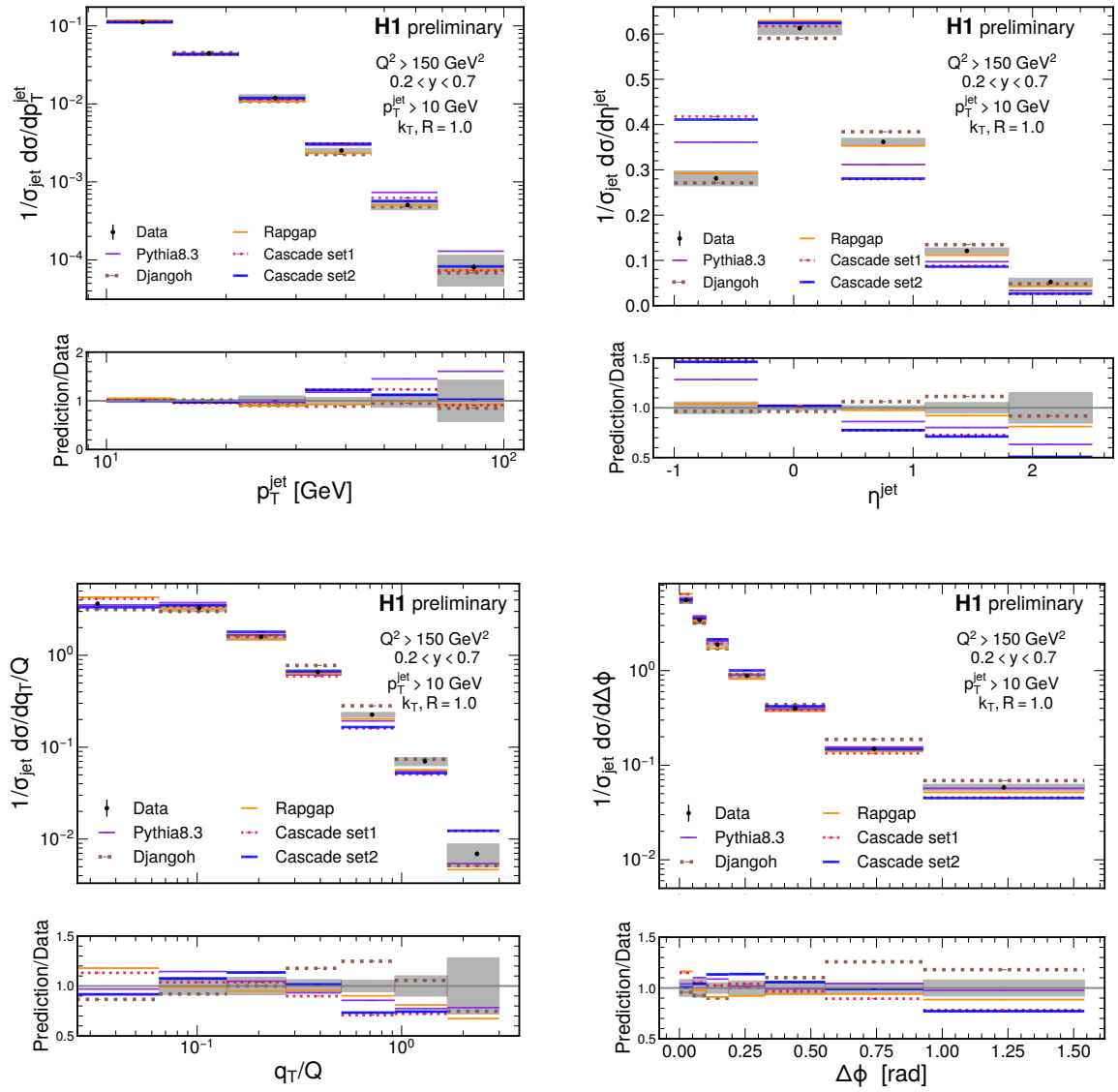

Fig. 6: Measured cross-sections, normalized to the inclusive jet production cross section, as a function of the jet transverse momentum, jet pseudorapidity, lepton-jet momentum balance, and lepton-jet azimuthal angle correlation. Predictions obtained with RAPGAP, DJANGOH, PYTHIA8.3, and CASCADE generators are shown as well. At the bottom, the ratio between predictions and the data are shown. The gray bands represent the total systematic uncertainty of the data; the bars represent the statistical uncertainty of the data, which is typically smaller than the marker size.

the LO calculation are significant, especially at low $p_{\mathrm{T}}^{\mathrm{jet}}$. The $\eta_{\mathrm{lab}}^{\mathrm{jet}}$ cross-section is not entirely described by either LO, NLO nor NNLO calculations. The trend of the deviations from data with increasing order indicates that N^{3}LO accuracy might be needed to describe the data. The q_T/Q spectrum is described by the NNLO calculation within uncertainties in the region $q_T/Q > 0.3$ but at lower values, the predictions deviate by more than a factor of 2.5. The TMD calculation, which includes resummation, describes the data from the low q_T to up to $q_T/Q \approx 1.0$, which is well beyond the assumed validity region of the TMD framework. Both the NLO and NNLO calculations describe the $\Delta\phi$ spectrum within uncertainties, except at low $\Delta\phi$ where non-physical trends are observed. The TMD calculation describes the data well for $\Delta\phi < 0.75$ radian.

RAPGAP describes the $p_{\mathrm{T}}^{\mathrm{jet}}$ and $\eta_{\mathrm{lab}}^{\mathrm{jet}}$ cross-sections within uncertainties, whereas DJANGOH describes the $p_{\mathrm{T}}^{\mathrm{jet}}$ cross-section within uncertainty and shows small but significant differences with the $\eta_{\mathrm{lab}}^{\mathrm{jet}}$ cross-section. PYTHIA8.3 describes the low $p_{\mathrm{T}}^{\mathrm{jet}}$ spectrum well but predicts a significantly harder $p_{\mathrm{T}}^{\mathrm{jet}}$ spectrum beyond about 30 GeV; it also deviates from the data significantly over the entire $\eta_{\mathrm{lab}}^{\mathrm{jet}}$ cross-section. The CASCADE calculations describe the $p_{\mathrm{T}}^{\mathrm{jet}}$ spectrum well but miss the $\eta_{\mathrm{lab}}^{\mathrm{jet}}$ shape; they also describe the data reasonable well at low q_T/Q and $\Delta\phi$ while missing the large values (likely due to missing higher-order contributions). In general, no event generator describes the q_T/Q and $\Delta\phi$ cross-sections over the entire range and significant deviations are observed especially at large q_T/Q or $\Delta\phi$, but overall they bracket the data for most of the measured range.

12 Conclusions

A measurements of jet production in DIS events with $Q^2 > 150$ GeV^2 and $0.2 < y < 0.7$ is presented. Jets are reconstructed in the laboratory frame with the k_{T} algorithm and $R = 1.0$. The following observables are measured: jet transverse momentum and pseudorapidity, as well as the TMD-sensitive observables q_{T}/Q (lepton-jet momentum balance) and $\Delta\phi$ (lepton-jet azimuthal angle correlation). The latter observables were recently motivated in Refs. [18, 21].

The jet transverse momentum spectra is well described by NNLO pQCD calculations; whereas the pseudorapidity is not described by NNLO calculations and hints that higher-order corrections are not small. The q_T/Q spectrum is well described by TMD calculations up to $q_T/Q \lesssim 1$. The pQCD calculations describe the large q_T region but diverge at low q_T/Q values, as expected. An overlap of the pure TMD and collinear QCD calculations is observed over a significant region of the q_T/Q spectrum, which indicates that these data could constrain the "matching" between the two frameworks. Similar conclusions follow from the $\Delta\phi$ spectrum.

Overall, the event generators included in this study describe all the measured distributions, including the q_T/Q and $\Delta\phi$, rather well. In fact, the predictions from event generators "bracket" the data over most kinematic intervals. The most significant discrepancies with the data are observed for PYTHIA8.3 at high p_{T}, as well as for the shape of the pseudorapidity distribution. This indicates that further tuning of the recent PYTHIA8.3 version may be needed for DIS.

This measurement establishes a benchmark for jet-based TMD studies in DIS. It is also the first measurement that uses machine-learning assisted unfolding, which was based on the recently proposed OMNIFOLD method [50]. This is the first measurement in a series of studies that aim at creating a pathfinder program for the future Electron-Ion Collider. Future work includes measurements of jet fragmentation and differential cross-sections as a function x and Q^2.

Bibliography

[1] Andrei V. Belitsky, Xiang-dong Ji, and Feng Yuan. Quark imaging in the proton via quantum phase space distributions. *Phys. Rev. D*, 69:074014, 2004.

[2] V. N. Gribov and L. N. Lipatov. Deep inelastic e p scattering in perturbation theory. *Sov. J. Nucl. Phys.*, 15:438–450, 1972.

[3] Yuri L. Dokshitzer. Calculation of the Structure Functions for Deep Inelastic Scattering and e+ e- Annihilation by Perturbation Theory in Quantum Chromodynamics. *Sov. Phys. JETP*, 46:641–653, 1977.

[4] Guido Altarelli and G. Parisi. Asymptotic Freedom in Parton Language. *Nucl. Phys. B*, 126:298–318, 1977.

[5] Markus A. Ebert, Iain W. Stewart, and Yong Zhao. Determining the Nonperturbative Collins-Soper Kernel From Lattice QCD. *Phys. Rev. D*, 99(3):034505, 2019.

[6] Phiala Shanahan, Michael Wagman, and Yong Zhao. Collins-Soper kernel for TMD evolution from lattice QCD. *Phys. Rev. D*, 102(1):014511, 2020.

[7] Harut Avakian, Bakur Parsamyan, and Alexey Prokudin. Spin orbit correlations and the structure of the nucleon. *Riv. Nuovo Cim.*, 42(1):1–48, 2019.

[8] Alessandro Bacchetta, Filippo Delcarro, Cristian Pisano, Marco Radici, and Andrea Signori. Extraction of partonic transverse momentum distributions from semi-inclusive deep-inelastic scattering, Drell-Yan and Z-boson production. *JHEP*, 06:081, 2017. [Erratum: JHEP 06, 051 (2019)].

[9] Daniel Boer and Werner Vogelsang. Asymmetric jet correlations in pp uparrow scattering. *Phys. Rev. D*, 69:094025, 2004.

[10] B. I. Abelev et al. Measurement of transverse single-spin asymmetries for di-jet production in proton-proton collisions at $\sqrt{s}$ = 200-GeV. *Phys. Rev. Lett.*, 99:142003, 2007.

[11] C.J. Bomhof, P.J. Mulders, W. Vogelsang, and F. Yuan. Single-transverse spin asymmetry in dijet correlations at hadron colliders. *Phys. Rev. D*, 75:074019, 2007.

[12] Leszek Adamczyk et al. Azimuthal transverse single-spin asymmetries of inclusive jets and charged pions within jets from polarized-proton collisions at $\sqrt{s} = 500$ GeV. *Phys. Rev. D*, 97(3):032004, 2018.

[13] Zhong-Bo Kang, Alexei Prokudin, Felix Ringer, and Feng Yuan. Collins azimuthal asymmetries of hadron production inside jets. *Phys. Lett. B*, 774:635–642, 2017.

[14] Umberto D'Alesio, Francesco Murgia, and Cristian Pisano. Testing the universality of the Collins function in pion-jet production at RHIC. *Phys. Lett. B*, 773:300–306, 2017.

[15] Roel Aaij et al. Measurement of charged hadron production in Z-tagged jets in proton-proton collisions at $\sqrt{s} = 8$ TeV. *Phys. Rev. Lett.*, 123(23):232001, 2019.

[16] Daniel Gutierrez-Reyes, Ignazio Scimemi, Wouter J. Waalewijn, and Lorenzo Zoppi. Transverse momentum dependent distributions with jets. *Phys. Rev. Lett.*, 121(16):162001, 2018.

[17] Daniel Gutierrez-Reyes, Ignazio Scimemi, Wouter J. Waalewijn, and Lorenzo Zoppi. Transverse momentum dependent distributions in e^+e^- and semi-inclusive deep-inelastic scattering using jets. *JHEP*, 10:031, 2019.

[18] Xiaohui Liu, Felix Ringer, Werner Vogelsang, and Feng Yuan. Lepton-jet correlations in deep inelastic scattering at the Electron-Ion Collider. *Phys. Rev. Lett.*, 122(19):192003, 2019.

[19] Zhong-Bo Kang, Kyle Lee, and Fanyi Zhao. Polarized jet fragmentation functions. *Phys. Lett. B*, 809:135756, 2020.

[20] Daniel Gutierrez-Reyes, Yiannis Makris, Varun Vaidya, Ignazio Scimemi, and Lorenzo Zoppi. Probing transverse-momentum distributions with groomed jets. *JHEP*, 08:161, 2019.

[21] Xiaohui Liu, Felix Ringer, Werner Vogelsang, and Feng Yuan. Lepton-jet correlation in deep inelastic scattering. *Phys. Rev. D*, 102(9):094022, 2020.

[22] Paul Newman and Matthew Wing. The hadronic final state at HERA. *Rev. Mod. Phys.*, 86(3):1037, 2014.

[23] Miguel Arratia, Yiannis Makris, Duff Neill, Felix Ringer, and Nobuo Sato. Asymmetric jet clustering in deep-inelastic scattering, arXiv:2006.10751.

[24] I. Abt et al. The H1 detector at HERA. 7 1993.

[25] K. Charchula, G. A. Schuler, and H. Spiesberger. Combined QED and QCD radiative effects in deep inelastic lepton - proton scattering: The Monte Carlo generator DJANGO6. *Comput. Phys. Commun.*, 81:381–402, 1994.

[26] Hannes Jung. Hard diffractive scattering in high-energy e p collisions and the Monte Carlo generator RAPGAP. *Comput. Phys. Commun.*, 86:147–161, 1995.

[27] R. Brun, F. Bruyant, M. Maire, A. C. McPherson, and P. Zanarini. GEANT3. 9 1987.

[28] Vladimir Andreev et al. Measurement of jet production cross sections in deep-inelastic ep scattering at HERA. *Eur. Phys. J. C*, 77(4):215, 2017.

[29] Ursula Bassler and Gregorio Bernardi. On the kinematic reconstruction of deep inelastic scattering at HERA: The Sigma method. *Nucl. Instrum. Meth. A*, 361:197–208, 1995.

[30] An energy flow algorithm for Hadronic Reconstruction in OO: Hadroo2, H1-01/05-616, https://marh1.in2p3.fr/doc/h1-0105-616.pdf2003.

[31] M Peez. Search for deviations from the standard model in high transverse energy processes at the electron proton collider HERA. (Dissertation, Univ. Lyon), 2003.

[32] F. D. Aaron et al. Inclusive deep inelastic scattering at high Q^2 with longitudinally polarised lepton beams at HERA. *JHEP*, 09:061, 2012.

[33] V. Andreev et al. Measurement of multijet production in ep collisions at high Q^2 and determination of the strong coupling α_s. *Eur. Phys. J. C*, 75(2):65, 2015.

[34] Miguel G. Echevarria, Zhong-Bo Kang, and John Terry. Global analysis of the Sivers functions at NLO+NNLL in QCD. *JHEP*, 01:126, 2021.

[35] J. Collins, L. Gamberg, A. Prokudin, T. C. Rogers, N. Sato, and B. Wang. Relating transverse momentum dependent and collinear factorization theorems in a generalized formalism. *Phys. Rev. D*, 94(3):034014, 2016.

[36] Matteo Cacciari, Gavin P. Salam, and Gregory Soyez. FastJet User Manual. *Eur. Phys. J. C*, 72:1896, 2012.

[37] Matteo Cacciari and Gavin P. Salam. Dispelling the N^3 myth for the k_t jet-finder. *Phys. Lett. B*, 641:57–61, 2006.

[38] S. Catani, Yuri L. Dokshitzer, M. H. Seymour, and B. R. Webber. Longitudinally invariant K_t clustering algorithms for hadron hadron collisions. *Nucl. Phys. B*, 406:187–224, 1993.

[39] Stephen D. Ellis and Davison E. Soper. Successive combination jet algorithm for hadron collisions. *Phys. Rev. D*, 48:3160–3166, 1993.

[40] G. D'Agostini. A Multidimensional unfolding method based on Bayes' theorem. *Nucl. Instrum. Meth.*, A362:487–498, 1995.

[41] Andreas Höcker and Vakhtang Kartvelishvili. SVD approach to data unfolding. *Nucl. Instrum. Meth.*, A372:469–481, 1996.

[42] Stefan Schmitt. TUnfold: an algorithm for correcting migration effects in high energy physics. *JINST*, 7:T10003, 2012.

[43] G. Zech and B. Aslan. Binning-free unfolding based on Monte Carlo migration. *eConf*, C030908:TUGT001, 2003. [,138(2003)].

[44] L. Lindemann and Gunter Zech. Unfolding by weighting Monte Carlo events. *Nucl. Instrum. Meth. A*, 354:516–521, 1995.

[45] Kaustuv Datta, Deepak Kar, and Debarati Roy. Unfolding with generative adversarial networks. 2018.

[46] Marco Bellagente, Anja Butter, Gregor Kasieczka, Tilman Plehn, Armand Rousselot, Ramon Winterhalder, Lynton Ardizzone, and Ullrich Köthe. Invertible networks or partons to detector and back again. 6 2020.

[47] Marco Bellagente, Anja Butter, Gregor Kasieczka, Tilman Plehn, and Ramon Winterhalder. How to GAN away detector effects. *SciPost Phys.*, 8(4):070, 2020.

[48] Nikolai D. Gagunashvili. Machine learning approach to inverse problem and unfolding procedure, arXiv:1004.2006.

[49] Alexander Glazov. Machine learning as an instrument for data unfolding, arXiv:1712.01814 .

[50] Anders Andreassen, Patrick T. Komiske, Eric M. Metodiev, Benjamin Nachman, and Jesse Thaler.

OmniFold: a method to simultaneously unfold all observables. *Phys. Rev. Lett.*, 124(18):182001, 2020.

[51] L. B. Lucy. An iterative technique for the rectification of observed distributions. *Astronomical Journal*, 79:745, June 1974.

[52] William Hadley Richardson. Bayesian-based iterative method of image restoration. *J. Opt. Soc. Am.*, 62(1):55–59, Jan 1972.

[53] Fraciois Chollet. Keras. https://github.com/fchollet/keras, 2017.

[54] Martín Abadi, Paul Barham, Jianmin Chen, Zhifeng Chen, Andy Davis, Jeffrey Dean, Matthieu Devin, Sanjay Ghemawat, Geoffrey Irving, Michael Isard, et al. Tensorflow: A system for large-scale machine learning. In *OSDI*, volume 16, pages 265–283, 2016.

[55] Diederik Kingma and Jimmy Ba. Adam: A method for stochastic optimization. 2014.

[56] Ignacio Borsa, Daniel de Florian, and Iván Pedron. Jet production in polarized deep inelastic scattering at next-to-next-to-leading order. *Phys. Rev. Lett.*, 125(8):082001, 2020.

[57] Ignacio Borsa, Daniel de Florian, and Iván Pedron. Inclusive-jet and dijet production in polarized deep inelastic scattering. *Phys. Rev. D*, 103(1):014008, 2021.

[58] Matteo Cacciari, Frédéric A. Dreyer, Alexander Karlberg, Gavin P. Salam, and Giulia Zanderighi. Fully Differential Vector-Boson-Fusion Higgs Production at Next-to-Next-to-Leading Order. *Phys. Rev. Lett.*, 115(8):082002, 2015. [Erratum: Phys.Rev.Lett. 120, 139901 (2018)].

[59] Peng Sun, Joshua Isaacson, C. P. Yuan, and Feng Yuan. Nonperturbative functions for SIDIS and Drell–Yan processes. *Int. J. Mod. Phys. A*, 33(11):1841006, 2018.

[60] Leif Lonnblad. ARIADNE version 4: A Program for simulation of QCD cascades implementing the color dipole model. *Comput. Phys. Commun.*, 71:15–31, 1992.

[61] J. Pumplin, D. R. Stump, J. Huston, H. L. Lai, Pavel M. Nadolsky, and W. K. Tung. New generation of parton distributions with uncertainties from global QCD analysis. *JHEP*, 07:012, 2002.

[62] Bo Andersson, G. Gustafson, G. Ingelman, and T. Sjostrand. Parton fragmentation and string dynamics. *Phys. Rept.*, 97:31–145, 1983.

[63] Torbjorn Sjöstrand, Stephen Mrenna, and Peter Z. Skands. PYTHIA 6.4 physics and manual. *JHEP*, 05:026, 2006.

[64] Torbjorn Sjöstrand, Stephen Mrenna, and Peter Z. Skands. A brief introduction to PYTHIA 8.1. *Comput. Phys. Commun.*, 178:852, 2008.

[65] Richard D. Ball et al. Parton distributions with LHC data. *Nucl. Phys. B*, 867:244–289, 2013.

[66] S. Baranov et al. CASCADE3 A Monte Carlo event generator based on TMDs. 1 2021.

[67] A. van Hameren. KaTie : For parton-level event generation with k_T-dependent initial states. *Comput. Phys. Commun.*, 224:371–380, 2018.

[68] A. Bermudez Martinez, P. Connor, H. Jung, A. Lelek, R. Žlebčík, F. Hautmann, and V. Radescu. Collinear and TMD parton densities from fits to precision DIS measurements in the parton branching method. *Phys. Rev. D*, 99(7):074008, 2019.

[69] F. Hautmann, H. Jung, A. Lelek, V. Radescu, and R. Zlebcik. Collinear and TMD Quark and Gluon Densities from Parton Branching Solution of QCD Evolution Equations. *JHEP*, 01:070, 2018.

[70] F. Hautmann, H. Jung, A. Lelek, V. Radescu, and R. Zlebcik. Soft-gluon resolution scale in QCD evolution equations. *Phys. Lett. B*, 772:446–451, 2017.

[71] H. Abramowicz et al. Combination of measurements of inclusive deep inelastic $e^{\pm}p$ scattering cross sections and QCD analysis of HERA data. *Eur. Phys. J. C*, 75(12):580, 2015.

[72] A. Bermudez Martinez et al. Production of Z-bosons in the parton branching method. *Phys. Rev. D*, 100(7):074027, 2019.

[73] A. Bermudez Martinez et al. The transverse momentum spectrum of low mass Drell–Yan production at next-to-leading order in the parton branching method. *Eur. Phys. J. C*, 80(7):598, 2020.

[74] Torbjörn Sjöstrand, Stefan Ask, Jesper R. Christiansen, Richard Corke, Nishita Desai, Philip Ilten, Stephen Mrenna, Stefan Prestel, Christine O. Rasmussen, and Peter Z. Skands. An introduction to PYTHIA 8.2. *Comput. Phys. Commun.*, 191:159–177, 2015.